X-ray spectra were measured using a silicon detector (XR-100CR, Amptek). We observed sharp K lines, and the characteristic x-ray intensities substantially increased with increases in the tube voltage (Figs, 10 and 12). Clean K lines were left by a 10-μm-thick copper filter, and the Kα lines were selected out by absorbing Kβ lines using a 10-μm-thick nickel filter (Figs. 11 and 13).

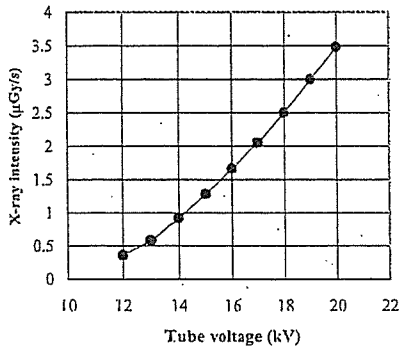

Fig. 6. X-ray intensity at 1.0 m from the pipe target according to changes in the tube voltage with a tube current of 0.10 mA.

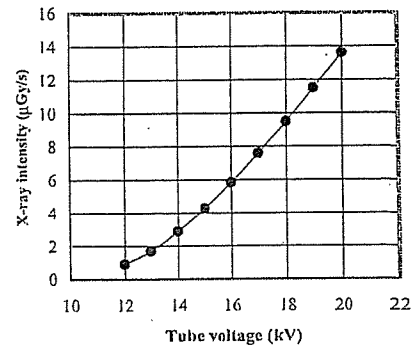

Fig. 7. X-ray intensity at 1.0 m from the rod target with changing the tube voltage with a tube current of 0.10 mA.

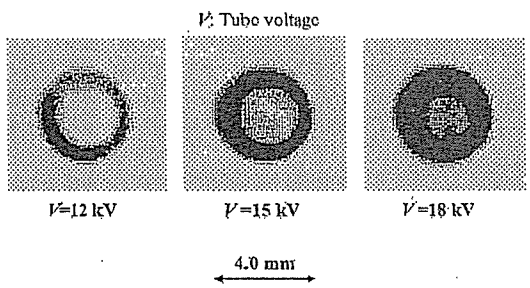

Fig. 8. Images of the characteristic x-ray source from the pipe target with changes in the tube voltage.

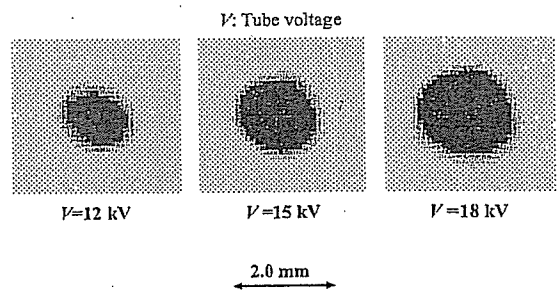

Fig. 9. Images of the characteristic x-ray source from the rod target.

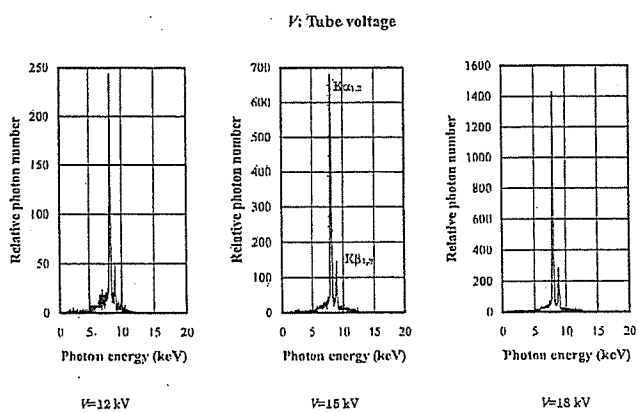

Fig. 10. X-ray spectra from the pipe target with changes in the tube voltage.

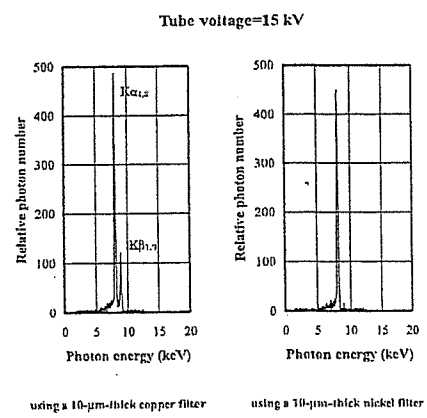

Fig. 11. X-ray spectra from the pipe target according to insertion of filters.

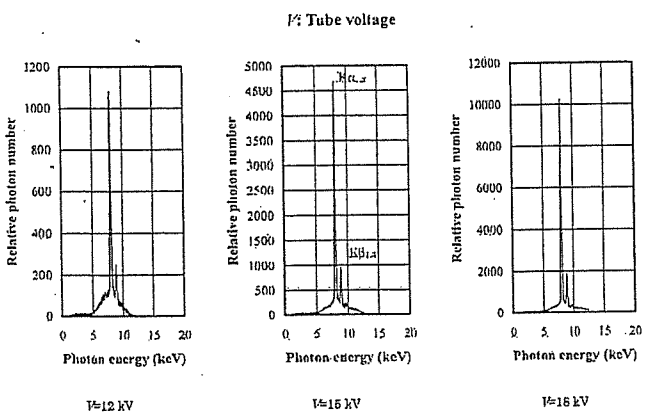

Fig. 12. X-ray spectra from the rod target with changing the tube voltage

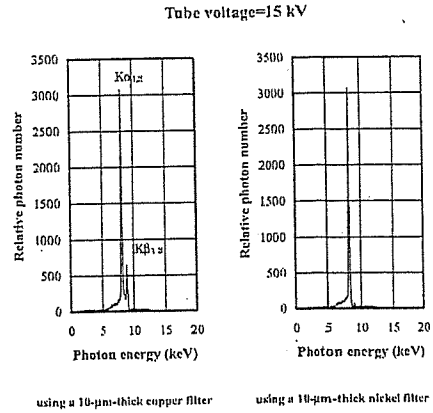

Fig. 13. X-ray spectra from the rod target according to insertion of filters.

4. CONCLUSIONS AND OUTLOOK

We developed a super-characteristic x-ray generator with the pipe and rod targets and succeeded in producing copper K lines. The characteristic x-ray intensity increased with increases in the tube voltage, and monochromatic Kα lines were left by the nickel filter.

In the spectrum measurements, we usually employ a silicon detector and a lithium fluoride curved crystal. The detector is useful for measuring the total spectra, including scattering beams. On the other hand, the spectra from only the x-ray source can be measured using the crystal by selecting Bragg's angle. Using the crystal in conjunction with a computed radiography system, we observed clean copper K lines.

In this preliminary experiment, although the maximum tube voltage and current were 20 kV and 0.10 mA, the voltage and current could be increased to 100 kV and 1.0 mA, respectively. Using the rod target, the generator produced maximum number of characteristic photons from the rod target was approximately 1×10^6 photons/(cm^2· s) at 1.0 m from the source, and the photon count rate can be increased easily by increasing the current.

Currently, the copper K-series characteristic x-rays are useful for extremely soft radiography, and the photon energies of characteristic x-rays can be selected by the target element. In particular, the pipe target is useful for forming monochromatic line beams by decreasing the bore diameter.

ACKNOWLEDGMENT

This work was supported by Grants-in-Aid for Scientific Research (13470154, 13877114, and 16591222) and Advanced Medical Scientific Research from MECSST, Health and Labor Sciences Research Grants (RAMT-nano-001, RHGTEFB-genome-005 and RHGTEFB-saisei-003), and grants from the Keiryo Research Foundation, Promotion and Mutual Aid Corporation for Private Schools of Japan, Japan Science and Technology Agency (JST), and New Energy and Industrial Technology Development Organization (NEDO, Industrial Technology Research Grant Program in '03).

REFERENCES

1. J.J. Rocca, V. Shlyaptsev, F.G. Tomasel, O.D.Cortazar, D. Hartshorn and J.L.A. Chilla, "Demonstration of a discharge pumped table-top soft x-ray laser," *Phys. Lev. Lett.*, 73, 2192-2195, 1994.

2. J.J.G. Rocca, J.L.A. Chilla, S. Sakadzic, A. Rahman, J. Filevich, E. Jankowska, E.C. Hammarsten, B.M. Luther, H.C. Kapteyn, M. Murnane and V.N. Shlyapsev, "Advances in capillary discharge soft x-ray laser research," *SPIE*, 4505, 1-6, 2001.

3. S. Le Pape, Ph. Zeitoun, J.J.G. Rocca, A. Carillon, P. Dhez, M. Francois, S. Hubert, M. Idir and D. Ros, "Characterisation of an x-ray laser beam," *SPIE*, 4505, 23-34, 2001.

4. C. Gerth, "Free-electron laser at the TESLA test facility at DESY: toward a tunable short-pulsed soft x-ray source," *SPIE*, 4505, 131-145, 2001.

5. E. Sato, Y. Hayasi, R. Germer, E. Tanaka, H. Mori, T. Kawai, T. Ichimaru, K. Takayama and H. Ido, "Quasi-monochromatic flash x-ray generator utilizing weakly ionized linear copper plasma," *Rev. Sci. Instrum.*, 74, 5236-5240, 2003.

6. E. Sato, Y. Hayasi, R. Germer, E. Tanaka, H. Mori, T. Kawai, T. Ichimaru, S. Sato, K. Takayama and H. Ido, "Sharp characteristic x-ray irradiation from weakly ionized linear plasma," *J. Electron Spectrosc. Related Phenom.*, 137-140, 713-720, 2004.

7. E. Sato, E. Tanaka, H. Mori, T. Kawai, S. Sato and K. Takayama, "Clean monochromatic x-ray irradiation from weakly ionized linear copper plasma," *Opt. Eng.*, 44, 049002-1-6, 2005.

8. E. Sato, Y. Hayasi, R. Germer, E. Tanaka, H. Mori, T. Kawai, T. Inoue, A. Ogawa, S. Sato, K. Takayama, J. Onagawa, "X-ray spectra from weakly ionized linear copper plasma," *Jpn. J. Appl. Phys.*, 45, 5301-5306, 2006.

9. E. Sato, M. Sagae, E. Tanaka, Y. Hayasi, R. Germer, H. Mori, T. Kawai, T. Ichimaru, S. Sato, K. Takayama and H. Ido, "Quasi-monochromatic flash x-ray generator utilizing a disk-cathode molybdenum tube," *Jpn. J. Appl. Phys.*, 43, 7324-7328, 2004.

10. E. Sato, E. Tanaka, H. Mori, T. Kawai, T. Ichimaru, S. Sato, K. Takayama and H. Ido, "Compact monochromatic flash x-ray generator utilizing a disk-cathode molybdenum tube," *Med. Phys.*, 32, 49-54, 2005.

11. E. Sato, Y. Hayasi, K. Kimura, E. Tanaka, H. Mori, T. Kawai, T. Inoue, A. Ogawa, S. Sato, K. Takayama, J. Onagawa and H. Ido, "Enhanced K-edge angiography utilizing tantalum plasma x-ray generator in conjunction with gadolium-based contrast media," *Jpn. J. Appl. Phys.*, 44, 8716-8721, 2005.

12. H. Mori, K. Hyodo, E. Tanaka, M. U. Mohammed, A. Yamakawa, Y. Shinozaki, H. Nakazawa, Y. Tanaka, T. Sekka, Y. Iwata, S. Honda, K. Umetani, H. Ueki, T. Yokoyama, K. Tanioka, M. Kubota, H. Hosaka, N. Ishizawa and M. Ando, "Small-vessel radiography in situ with monochromatic synchrotoron radiation," *Radiology*, 201, 173-177, 1996.

13. K. Hyodo, M. Ando, Y. Oku, S. Yamamoto, T. Takeda, Y. Itai, S. Ohtsuka, Y. Sugishita and J. Tada, "Development of a two-dimensional imaging system for clinical applications of intravenous coronary angiography using intense synchrotron radiation produced by a multipole wiggler," *J. Synchrotron Radiat.*, 5, 1123-1126, 1998.

14. E. Sato, E. Tanaka, H. Mori, T. Kawai, T. Ichimaru, S. Sato, K. Takayama and H. Ido, "Demonstration of enhanced K-edge angiography using a cerium target x-ray generator," *Med. Phys*, 31, 3017-3021, 2004.

15. E. Sato, A. Yamadera, E. Tanaka, H. Mori, T. Kawai, F. Ito, T. Inoue, A. Ogawa, S. Sato, K. Takayama, J. Onagawa and H. Ido, "X-ray spectra from a cerium target and their application to cone beam K-edge angiography," *Opt. Eng.*, 44, 096502-1-6, 2005.

16. E. Sato, E. Tanaka, H. Mori, T. Kawai, T. Inoue, A. Ogawa, A. Yamadera, S. Sato, F. Ito, K. Takayama, J. Onagawa and H. Ido, "Variations in cerium x-ray spectra and enhanced K-edge angiography," *Jpn. J. Appl. Phys.*, 44, 8204-8209, 2005.

*dresato@iwate-med.ac.jp; phone +81-19-651-5111; fax +81-19-654-9282

Japanese Journal of Applied Physics
Vol. 45, No. 4A, 2006, pp. 2845–2849

Characteristic X-ray Generator Utilizing Angle Dependence of Bremsstrahlung X-ray Distribution

Eiichi SATO, Etsuro TANAKA[1], Hidezo MORI[2], Toshiaki KAWAI[3], Takashi INOUE[4], Akira OGAWA[4], Shigehiro SATO[5], Kazuyoshi TAKAYAMA[6] and Jun ONAGAWA[7]

Department of Physics, Iwate Medical University, 3-16-1 Honchodori, Morioka 020-0015, Japan
[1]*Department of Nutritional Science, Faculty of Applied Bio-science, Tokyo University of Agriculture, 1-1-1 Sakuragaoka, Setagaya-ku, Tokyo 156-8502, Japan*
[2]*Department of Cardiac Physiology, National Cardiovascular Center Research Institute, 5-7-1 Fujishirodai, Suita, Osaka 565-8565, Japan*
[3]*Electron Tube Division #2, Hamamatsu Photonics K.K., 314-5 Shimokanzo, Iwata, Shizuoka 438-0193, Japan*
[4]*Department of Neurosurgery, School of Medicine, Iwate Medical University, 19-1 Uchimaru, Morioka 020-8505, Japan*
[5]*Department of Microbiology, School of Medicine, Iwate Medical University, 19-1 Uchimaru, Morioka 020-8505, Japan*
[6]*Shock Wave Research Center, Institute of Fluid Science, Tohoku University, 2-1-1 Katahira, Sendai 980-8577, Japan*
[7]*Department of Applied Physics and Informatics, Faculty of Engineering, Tohoku Gakuin University, 1-13-1 Chuo, Tagajo, Miyagi 985-8537, Japan*

(Received November 17, 2005; revised December 24, 2005; accepted December 31, 2005; published online April 7, 2006)

This generator consists of the following components: a constant high-voltage power supply, a filament power supply, a turbomolecular pump, and an X-ray tube. The X-ray tube is a demountable diode which is connected to the turbomolecular pump and consists of the following major devices: a molybdenum rod target, a tungsten hairpin cathode (filament), a focusing (Wehnelt) electrode, a polyethylene terephthalate X-ray window 0.25 mm in thickness, and a stainless-steel tube body. In the X-ray tube, the positive high voltage is applied to the anode (target) electrode, and the cathode is connected to the tube body (ground potential). In this experiment, the tube voltage applied was from 22 to 36 kV, and the tube current was regulated to within 100 μA by the filament temperature. The exposure time is controlled in order to obtain optimum X-ray intensity. The electron beams from the cathode are converged to the target by the focusing electrode, and clean K-series characteristic X-rays are produced through the focusing electrode without using a filter. The X-ray intensity was 26.6 μGy/s at 1.0 m from the X-ray source with a tube voltage of 30 kV and a tube current of 100 μA, and quasi-monochromatic radiography was performed using a computed radiography system. [DOI: 10.1143/JJAP.45.2845]

KEYWORDS: demountable X-ray tube, electron-impact source, quasi-monochromatic X-rays, K-series characteristic X-rays, Sommerfeld's theory

1. Introduction

A great deal of effort has been devoted to the research and development of X-ray lasers in past years, and several different generators have been developed. Using tera-watt pulse lasers as pumping sources, a transient collisional excitation method has been proposed.[1] Subsequently, capillary discharge soft X-ray laser generators[2–4] have been developed and demonstrated. However, it is difficult to produce high-photon-energy X-ray lasers with energies 10 keV or beyond.

Recently, we have developed several different flash X-ray generators[5–9] corresponding to specific radiographic objectives, and the plasma X-ray source has been growing with increases in the electrostatic energy in the condenser. By forming weakly ionized linear plasma using rod targets, we confirmed irradiation of clean K-series characteristic X-rays such as hard X-ray lasers from the plasma axial direction using a table-top flash X-ray generator.[10–13] This super fluorescence has been employed to perform cone-beam monochromatic radiography such as iodine K-edge and gadolinium K-edge angiographies. Furthermore, because higher harmonic hard X-rays have been produced from the copper plasma, we have to confirm the irradiations of higher harmonics with charges in the target element.

Without forming plasmas, demountable flash X-ray tubes can be employed to perform fundamental study on producing monochromatic X-rays,[14] and have succeeded in producing clean K-series characteristic X-rays. However, monochromatic flash radiography has had difficulties in controlling X-ray duration, and in performing magnification radiography including phase-contrast effect.

At present, brilliant monochromatic parallel X-ray beams from synchrotron radiation are used in various fields including medical imaging,[15–17] and large-scale X-ray free electron laser sources[18] are constructing as a new-generation radiation source for producing monochromatic coherent X-rays. In contrast, small-scale steady-state monochromatic parallel and cone beams can be employed to perform medical imaging including phase-contrast radiography and K-edge angiography[19] in hospitals.

In this paper, we developed an X-ray generator used to perform a preliminary experiment for generating clean K-series characteristic X-rays by angle dependence of the bremsstrahlung X-rays.

2. Generator

Figure 1 shows a block diagram of a compact characteristic (quasi-monochromatic) X-ray generator. This generator consists of the following components: a constant high-voltage power supply (SL150, Spellman), a DC filament power supply, a turbomolecular pump, and an X-ray tube. The structure of the X-ray tube is illustrated in Fig. 2. The X-ray tube is a demountable diode which is connected to the turbomolecular pump with a pressure of approximately 0.5 mPa and consists of the following major devices: a molybdenum rod target of 3.0 mm in diameter, a tungsten hairpin cathode (filament), a focusing (Wehnelt) electrode, a polyethylene terephthalate X-ray window 0.25 mm in thickness, and a stainless-steel tube body. In the X-ray tube, the positive high voltage is applied to the anode (target) electrode, and the cathode is connected to the tube body

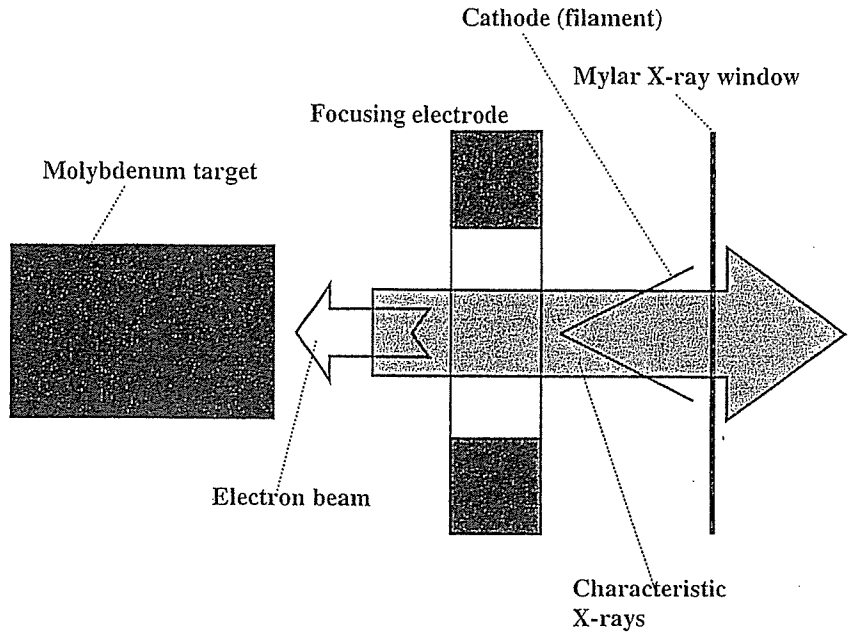

Fig. 3. K-photon irradiation from the X-ray tube.

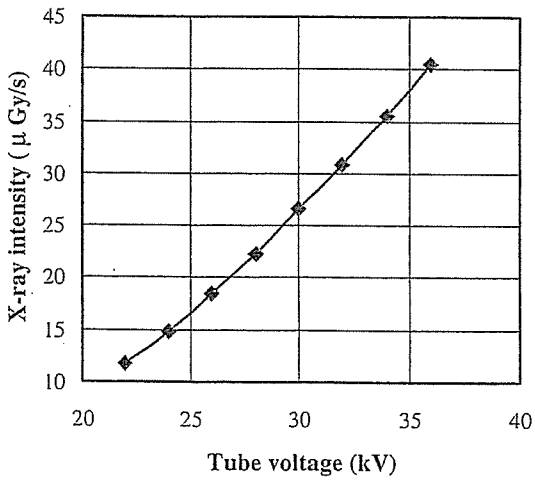

Fig. 4. X-ray intensity at 1.0 m from the X-ray source according to changes in the tube voltage with a tube current of 100 μA.

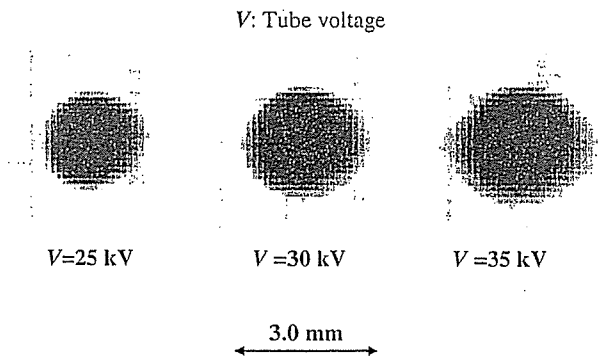

Fig. 5. Images of the characteristic X-ray source obtained using a pinhole camera with changes in the tube voltage.

detected by an imaging plate of the CR system (Konica Minolta, Regius 150) with a wide dynamic range, and relative X-ray intensity was calculated from Dicom original digital data corresponding to X-ray intensity; the data was scanned by Dicom viewer in the film-less CR system. Subsequently, the relative X-ray intensity as a function of the data was calibrated using a conventional X-ray generator, and we confirmed that the intensity was proportional to the exposure time. Figure 6 shows measured spectra from the molybdenum target. We observed clean K lines, while bremsstrahlung rays were hardly detected. The characteristic X-ray intensity substantially increased with increases in the tube voltage.

4. Radiography

The quasi-monochromatic radiography was performed by the CR system at 1.0 m from the X-ray source with the filter, and the tube voltage was 30 kV.

Firstly, rough measurements of image resolution were made using wires. Figure 7 shows radiograms of tungsten wires coiled around pipes made of poly(methyl methacrylate) (PMMA). Although the image contrast increased with increases in the wire diameter, a 50 μm-diameter wire could be observed.

A radiogram of a vertebra is shown in Fig. 8, and the fine structure of the vertebra was observed. Next, angiography was performed using iodine microspheres of 15 μm in diameter. Figures 9 and 10 show angiograms of a rabbit heart and thigh, respectively, and we could obtained high contrast images of coronary arteries and fine blood vessels.

5. Conclusions and Outlook

In summary, we developed a new quasi-monochromatic X-ray generator with a molybdenum-target tube and succeeded in producing clean molybdenum K lines. The characteristic X-ray intensity increased with increases in the tube voltage, and monochromatic Kα rays were left by a zirconium filter.

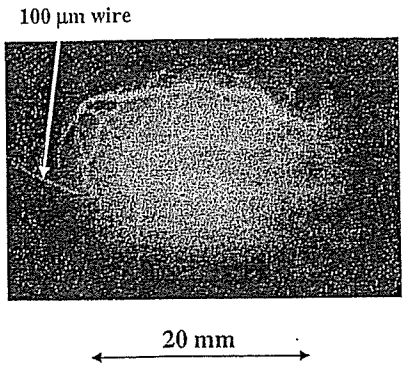

Fig. 9. Angiograms of a rabbit heart. Coronary arteries were visible.

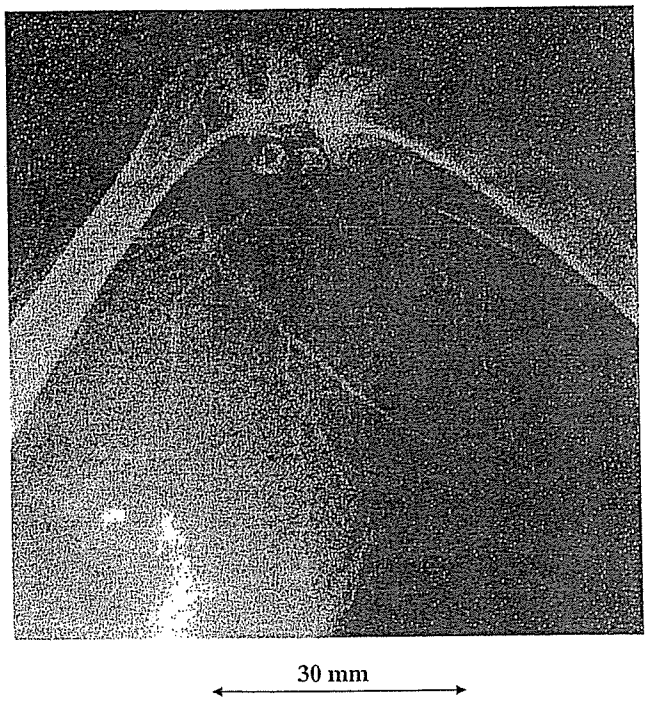

Fig. 10. Angiogram of a rabbit thigh. Fine blood vessels of approximately 100 μm were visible.

the target evaporation. Subsequently, the generator produced maximum number of characteristic photons was approximately 1×10^8 photons/(cm^2·s) at 1.0 m from the source, and the photon count rate can be increased easily by increasing the current.

In the present research, the molybdenum K-series characteristic X-rays are useful for mammography, and the photon energies of characteristic X-rays can be selected by the target element. In particular, enhanced K-edge angiography can be performed using a cerium target because cerium Kα rays (34.6 keV) are absorbed easily by iodine-based contrast media with an iodine K-edge of 33.2 keV. Using this angiography, coronary arteries and fine blood vessels formed in regenerative medicine may be observed with high contrasts. Furthermore, a flat panel detector is useful to observe blood flows for cases of cardiovascular disease.

Acknowledgment

This work was supported by Grants-in-Aid for Scientific Research (13470154, 13877114, and 16591222) and Advanced Medical Scientific Research from MECSST, Grants from Keiryo Research Foundation, The Promotion and Mutual Aid Corporation for Private School of Japan, JST (Test of Fostering Potential), NEDO, and MHLW (HLSRG, RAMT-nano-001, RHGTEFB-genome-005, and RGCD13C-1).

1) K. Nagashima, M. Tanaka, M. Nishikino, M. Kishimoto, M. Kado, T. Kawachi, N. Hasegawa, Y. Ochi, K. Sukegawa, R. Tai and K. Kato: Proc. SPIE **5197** (2003) 1.
2) J. J. Rocca, V. Shlyaptsev, F. G. Tomasel, O. D. Cortazar, D. Hartshorn and J. L. A. Chilla: Phys. Rev. Lett. **73** (1994) 2192.
3) C. D. Macchietto, B. R. Benware and J. J. Rocca: Opt. Lett. **24** (1999) 1115.
4) J. J. G. Rocca, J. L. A. Chilla, S. Sakadzic, A. Rahman, J. Filevich, E. Jankowska, E. C. Hammarsten, B. M. Luther, H. C. Kapteyn, M. Murnane and V. N. Shlyapsev: Proc. SPIE **4505** (2001) 1.
5) E. Sato, S. Kimura, S. Kawasaki, H. Isobe, K. Takahashi, Y. Tamakawa and T. Yanagisawa: Rev. Sci. Instrum. **61** (1990) 2343.
6) K. Takahashi, E. Sato, M. Sagae, T. Oizumi, Y. Tamakawa and T. Yanagisawa: Jpn. J. Appl. Phys. **33** (1994) 4146.
7) E. Sato, K. Takahashi, M. Sagae, S. Kimura, T. Oizumi, Y. Hayasi, Y. Tamakawa and T. Yanagisawa: Med. Biol. Eng. Comput. **32** (1994) 289.
8) E. Sato, M. Sagae, K. Takahashi, A. Shikoda, T. Oizumi, Y. Hayasi, Y. Tamakawa and T. Yanagisawa: Med. Biol. Eng. Comput. **32** (1994) 295.
9) E. Sato, E. Tanaka, H. Mori, T. Kawai, T. Ichimaru, S. Sato, K. Takayama and H. Ido: Med. Phys. **32** (2005) 49.
10) E. Sato, Y. Hayasi, R. Germer, E. Tanaka, H. Mori, T. Kawai, T. Ichimaru, K. Takayama and H. Ido: Rev. Sci. Instrum. **74** (2003) 5236.
11) E. Sato, Y. Hayasi, R. Germer, E. Tanaka, H. Mori, T. Kawai, T. Ichimaru, S. Sato, K. Takayama and H. Ido: J. Electron Spectrosc. Relat. Phenom. C **137–140** (2004) 713.
12) E. Sato, E. Tanaka, H. Mori, T. Kawai, S. Sato and K. Takayama: Opt. Eng. **44** (2005) 049002.
13) E. Sato, R. Germer, E. Tanaka, H. Mori, T. Kawai, T. Ichimaru, S. Sato, H. Ojima, K. Takayama and H. Ido: Proc. SPIE **5580** (2005) 146.
14) E. Sato, M. Sagae, E. Tanaka, Y. Hayasi, R. Germer, H. Mori, T. Kawai, T. Ichimaru, S. Sato, K. Takayama and H. Ido: Jpn. J. Appl. Phys. **43** (2004) 7324.
15) A. Momose, T. Takeda, Y. Itai and K. Hirano: Nat. Med. **2** (1996) 473.
16) H. Mori *et al.*: Radiology **201** (1996) 173.
17) K. Hyodo, M. Ando, Y. Oku, S. Yamamoto, T. Takeda, Y. Itai, S. Ohtsuka, Y. Sugishita and J. Tada: J. Synchrotron Radiat. **5** (1998) 1123.
18) K. Lan, E. E. Fill and J. M. Vehn: Proc. SPIE **5197** (2003) 253.
19) E. Sato, E. Tanaka, H. Mori, T. Kawai, T. Ichimaru, S. Sato, K. Takayama and H. Ido: Med. Phys. **31** (2004) 3017.
20) B. K. Agarwal: *X-ray Spectroscopy* (Springer-Verlag, New York, 1991) 2nd ed., p. 18.
21) E. Sato, K. Sato and Y. Tamakawa: Annu. Rep. Iwate Med. Univ. School Lib. Arts Sci. **35** (2000) 13.

Summary: An amphiphilic poly(*N*-propargylamide) with galactose and lauryloyl groups was synthesized by copolymerization of the corresponding *N*-propargylamide monomers using a Rh catalyst. The obtained copolymer formed a one-handed helical conformation and molecular aggregates in water. The observations by fluorescence microscopy in a cell culture experiment in the presence of dye-labeled copolymer indicated that the copolymer was incorporated into the cells.

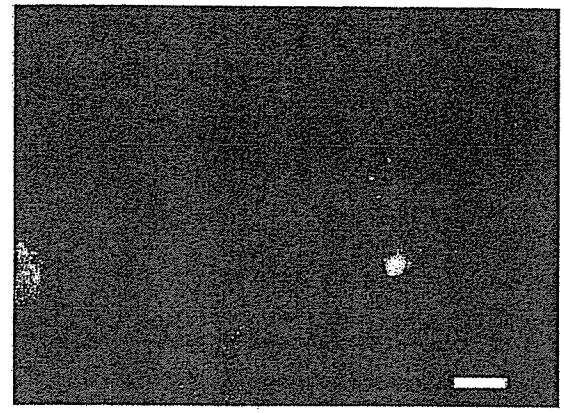

Localization of rhodamine B-labeled copolymer **8** in human aortic endothelial cells (fluorescence image).

Amphiphilic Poly(*N*-propargylamide) with Galactose and Lauryloyl Groups: Synthesis and Properties

Masakazu Suenaga,[1] *Yoshiro Kaneko,*[1] *Jun-ichi Kadokawa,**[1] *Takehiro Nishikawa,*[2] *Hideo Mori,*[2] *Masayoshi Tabata*[3]

[1]Department of Nanostructured and Advanced Materials, Graduate School of Science and Engineering, Kagoshima 890-0065, Japan
Fax: +81-99-285-3253; E-mail: kadokawa@eng.kagoshima-u.ac.jp
[2]National Cardiovascular Center, Suita, Osaka 565-8565, Japan
[3]Department of Molecular Chemistry, Graduate School of Engineering, Hokkaido University, Sapporo 060-8628, Japan

Received: July 19, 2006; Accepted: October 10, 2006; DOI: 10.1002/mabi.200600228

Keywords: amphiphiles; conjugated polymers; copolymerization; dynamic light scattering; nanoparticles; polyacetylenes

Introduction

Synthesis of polymers having sugar residues, so-called glycopolymers, has been widely investigated to seek biological applications because of their versatile functions.[1,1] It has been demonstrated that these glycopolymers can bind specifically to carbohydrate-recognition proteins, toxins, viruses, and cells, and, thus, these polymers can be utilized as cell culture substrates with specific cell recognition sites, as well as in targeting drug delivery systems.[2] The clustered saccharide ligands conjugated to the polymeric main chains are involved in these specific recognition processes. Most of the previously prepared glycopolymers have been based on a flexible polymer backbone, such as polystyrene and polyacrylamide.[3,4] This flexible nature of the glycopolymers causes the disordered orientation of the sugar residues in the glycopolymers. Regular orientation of the sugar residues is necessary for efficient interaction between the glycopolymers and receptor molecules. In this sense, the spatially regulated orientation of the sugar residues should be realized by attaching the sugar residues to a polymer backbone with a rigid conformation. The sugar residues attached to the rigid polymer backbone may give rise to the ordered orientation that can improve the molecular recognition of sugar residues by specific cell receptors. This is because the spatial regulation of the sugar residues is significant in molecular recognition as well as the chemical structure of the sugar molecules.[5]

From the above viewpoints, rigid glycopolymers with π-conjugated polymer backbones would be a novel type of bio-inspired polymers, which could exhibit multiple valence states and interact specifically and firmly with targets such as cell surface receptors and biomacromolecules. In some previous works, rigid glycopolymers having various π-conjugated main chains, such as polythiophene,[6] poly(*p*-phenylene ethynylene),[7] polyisocyanide,[8] polyaniline,[9] poly(*p*-phenylene vinylene),[10] and poly(phenylacetylene), have already been synthesized.[11] In the series of these studies, we reported the synthesis of poly(*N*-propargylamide) (**2**) with sugar residues. It contained a *cis*-polyacetylene main chain and was obtained by the rhodium-catalyzed polymerization of a *N*-propargylamide monomer (**1**) that had a galactose residue (Scheme 1).[12] Since polymerizations of the *N*-propargylamide monomers having various substituted groups using Rh catalyst have been widely reported to produce the corresponding poly(*N*-propargylamide) derivatives with *cis*-isomers,[13] we also investigated the copolymerization of **1** with *N*-propargylamide derivative **3** having a hexanoyl group to produce the amphiphilic glycopolymer **4**, as shown in Scheme 1. We tested the solubility of copolymer **4** in various solvents to confirm whether the copolymer exhibits an amphiphilic property. Although the homopolymer **2** is insoluble in common organic solvents, the copolymer **4** can be dissolved in some polar organic solvents, such as dimethyl sulfoxide (DMSO) and *N,N*-dimethylformamide (DMF), as well as in aqueous medium. However, the copolymer still exhibits a hydrophilic nature rather than an amphiphilic nature. We assumed that insufficient amphiphilicity of copolymer **4** could be attributed to poor hydrophobic property of the hydrophobic part.

In this study, we chose a more hydrophobic monomer: *N*-propargylamide monomer **5** having a longer alkyl chain, i.e., the lauryloyl group, as the hydrophobic part of the amphiphilic copolymer. The monomer **5** was copolymerized with **1** in the presence of Rh catalyst to give the corresponding amphiphilic copolymer **6** (Scheme 2). The resulting copolymer **6** can be expected to have the ability to conduct molecular aggregation in water, which is driven by intermolecular and intramolecular association of the hydrophobic lauryloyl groups.

We believe that such molecular aggregates of the amphiphilic copolymer should play a significant role in the field of targeted drug delivery. The idea is supported by the following characteristics of the molecular aggregates:

1) Drug carriers with nanometer dimensions can be obtained by molecular aggregation of amphiphilic copolymers.
2) Nano-sized aggregates can remain in the bloodstream for an extended period because of the size-dependent uptake in the reticuloendothelial system.
3) Drug molecules with hydrophobic natures can be loaded into hydrophobic milieus formed by the association of hydrophobic long alkyl chains; otherwise the drug molecules could be directly attached to the constituent monomer molecules of the copolymer.
4) Sugar residues of the copolymer can function as recognition sites for target cells and tissues as well as providing the hydrophilic character of the amphiphilic copolymer.

Therefore, we studied the *in vitro* cell uptake of the molecular aggregates of the amphiphilic copolymer. For this purpose, the fluorescent marker, rhodamine B, was introduced into the amphiphilic copolymer. In this article, we report the synthesis of the amphiphilic

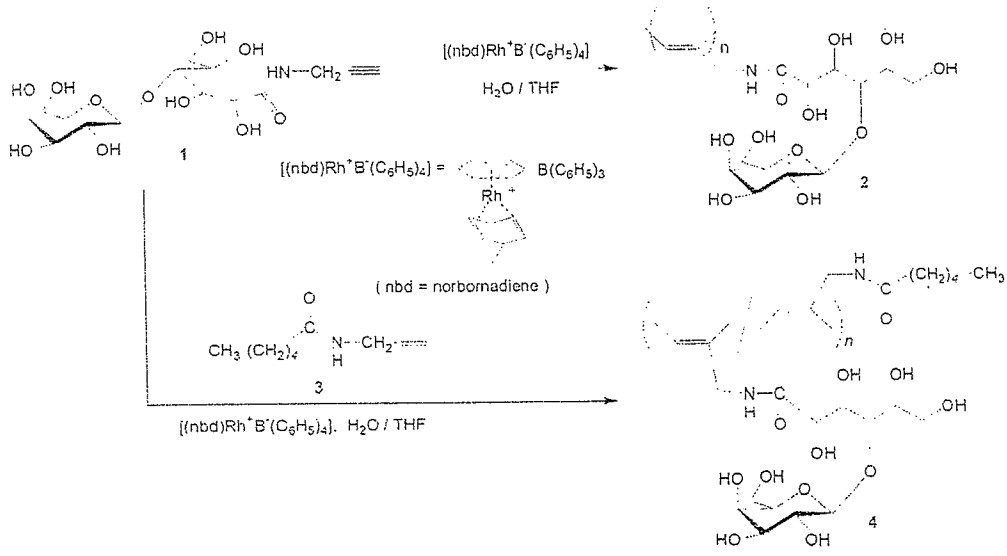

Scheme 1. Polymerization of **1** and copolymerization of **1** with **3**.

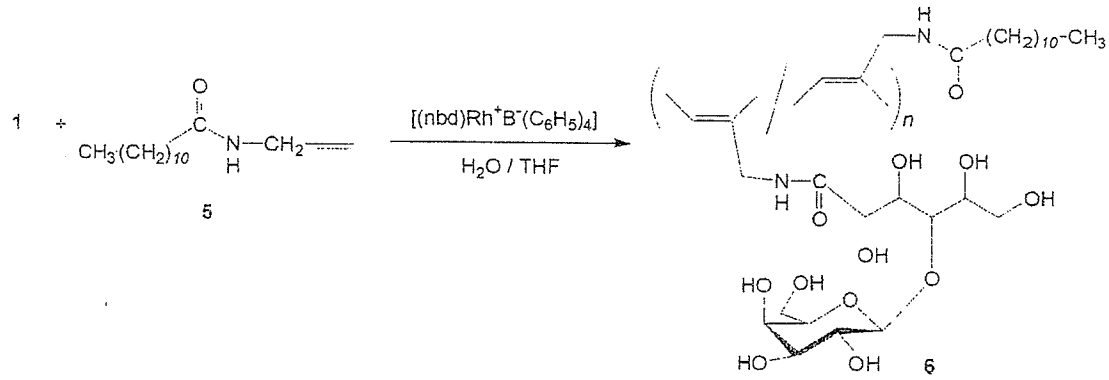

Scheme 2. Copolymerization of 1 with 5.

poly(*N*-propargylamide) **6** by Rh-catalyzed copolymerization, evaluation of its molecular aggregation in water [gel permeation chromatography (GPC) characterization, scanning electron microscopy (SEM) observation, and dynamic light scattering (DLS) measurement] and secondary conformation [circular dichroism (CD) spectra], and cell uptake of the nanoaggregate of the rhodamine-labeled amphiphilic copolymer (fluorescence microscopy).

Experimental Part

Materials

Monomer **1** and catalyst (nbd)Rh$^+$B$^-$ $(C_6H_5)_4$ were prepared according to the literature.[12,14] Tetrahydrofuran (THF) used as polymerization solvent was purified by distillation. Other reagents and solvents were used as received without further purification.

Synthesis of Monomer 5

Monomer **5** was synthesized by a method similar to that used for **3**.[15] Under argon, *N*-propargylamine hydrochloride (0.915 g, 10.0 mmol) was dissolved by slight warming in anhydrous acetonitrile (12.0 mL), and triethylamine (3.35 mL, 24.0 mmol) was added to the solution at room temperature. Then a solution of lauryloyl chloride (2.36 mL, 10.0 mmol) in anhydrous acetonitrile (12.0 mL) was added dropwise to the solution. After the mixture was stirred for 2 h, the reaction solution was concentrated by evaporation. The residue was dissolved in ethyl acetate and the solution was washed successively three times with 2 mol·L^{-1} hydrochloric acid and with saturated $NaHCO_3$ aqueous solution. The organic layer was dried over anhydrous Na_2SO_4, filtered, and evaporated. The residue was subjected to column chromatography on silica gel (hexane:ethyl acetate = 4:1, v/v) to isolate **5** (1.38 g, 5.82 mmol) in 58.2% yield.

^{1}H NMR ($CDCl_3$): $\delta = 0.88$ (t, $J = 7.2$ Hz, CH_3, 3H), 1.28 [m, $CH_3(CH_2)_8$, 16H], 1.62 (m, $CH_2CH_2C{=}O$, 2H), 2.19 (t, $J = 7.8$ Hz, $CH_2C{=}O$, 2H), 2.23 (t, $J = 2.4$ Hz, H–C≡C, 1H), 4.05–4.06 (m, CH_2N, 2H), 5.57 (s, NH, 1H).

Synthesis of Monomer 7

Under argon, triethylamine (0.836 mL, 6.00 mmol) was added to a solution of *N*-propargylamine hydrochloride (0.549 g, 6.00 mmol) and rhodamine B (1.92 g, 4.0 mmol) in anhydrous methanol (10.0 mL) at 0 °C. To the solution was added 1-[(3-dimethylamino)propyl]-3-ethylcarbodiimide hydrochloride (1.15 g, 6.00 mmol) as a condensing agent at 0 °C and the mixture was stirred for 17 h at room temperature. The precipitated material was isolated by filtration and dried under the reduced pressure to give **7** (0.472 g, 0.915 mmol) in 23.0% yield.

^{1}H NMR ($CDCl_3$): $\delta = 1.16$ (m, CH_3, 12H), 1.77 (t, $J =$ 2.4 Hz, H–C≡C, 1H), 3.33 (m, NCH_2CH_3, 8H), 3.95 (d, $J = 1.8$ Hz, $CH_2C{\equiv}$, 2H), 6.26–7.93 (m, aromatics, 10H).

Copolymerization of 1 with 5

A typical copolymerization procedure was as follows (entry 1, Table 1). Under argon, a solution of **5** (0.0356 g, 0.150 mmol) in THF (0.90 mL) and a solution of catalyst (0.00630 g, 0.0125 mmol) in THF (0.90 mL) were added to a solution of **1** (0.0397 g, 0.100 mmol) in water (0.20 mL) in this order at 30 °C. After the mixture was stirred at 30 °C for 140 min, the reaction mixture was concentrated by evaporation and dried under reduced pressure. The residue was dissolved in a small amount of DMSO and the solution was poured into a large amount of methanol to precipitate the polymeric product. The precipitate was isolated by filtration and was dried under reduced pressure to give **6** (0.0588 g) in 78.1% yield.

^{1}H NMR (DMSO-d_6): $\delta = 0.84$ (CH_3), 1.21 [$CH_3(CH_2)_8$], 1.45 ($CH_2CH_2C{=}O$), 2.15 ($CH_2C{=}O$), 3.0–3.9 [–CH(O–D-gal)–CH(OH)–CH_2OH, =CCH_2–, H2–H6 of D-gal], 4.04 [C(=O)CH(OH)CH(OH)–], 4.29 [C(=O)CH(OH)– and H1(β) of D-gal], 4.55, 4.79, 5.22 (OH), 6.11 (–CH=C–), 7.93 (NH).

Copolymerization of 1, 5, and 7

Under argon, a solution of **5** (0.0285 g, 0.120 mmol) and **7** (0.0929 g, 0.180 mmol) in THF (0.90 mL) and a solution of catalyst (0.0166 g, 0.0330 mmol) in THF (0.90 mL) were

Table 1. Results for copolymerization of 1 with 5 with Rh catalyst in THF–water (9:1) solvent.

Entry	Feed ratio[a]	Time	Yield[b]	Unit ratio[c]	$\overline{M}_n$[d]	$\overline{M}_w/\overline{M}_n$[d]	$[\alpha]_D$[e]
	1:5	min	%	1:5			degrees
1	1.0:1.5	140	78.1	1.0:0.92	9 100	1.30	
2	1.0:1.0	195	62.5	1.0:0.88	6 200	1.63	
3	1.0:0.67	240	57.0	1.0:0.35	5 200	1.60	−96.8
4	1.0:0.50	260	68.9	1.0:0.32	9 600	1.64	−142.3
5	1.0:0.33	200	69.9	1.0:0.26	7 100	1.50	−173.6
6	1.0:0.20	210	78.1	1.0:0.17	9 700	1.30	−185.6

[a] [Catalyst]/[1 + 5] = 0.05, reaction temperature: 30 °C.
[b] Fraction insoluble in methanol.
[c] Determined from ^{1}H NMR spectra.
[d] Determined by GPC with water as eluent using pullulan standards, sample concentration = 0.1 mg·mL^{-1}.
[e] Measured by polarimetry in water, c = 1.0 g·dL^{-1} at 20 °C.

added to a solution of 1 (0.143 g, 0.360 mmol) in water (0.20 mL) in this order at 30 °C. After the mixture was stirred at 30 °C for 18 h, the reaction mixture was concentrated by evaporation and dried under reduced pressure. The residue was dissolved in a small amount of DMSO and the solution was poured into a large amount of methanol to precipitate the polymeric product. The precipitate was isolated by filtration and dried under reduced pressure to give **8** (0.164 g) in 62.0% yield.

^{1}H NMR (DMSO-d_6 + D_2O): δ = 0.93 ($CH_3CH_2CH_2$), 1.16 (CH_3CH_2N), 1.25 [$CH_3(CH_2)_8$], 1.50 ($CH_2CH_2C{=}O$), 3.0–4.5 (sugar protons and =C–CH_2), 6.16 (HC=), 7.0–8.0 (aromatics).

Cell Culture Experiment

Human aortic endothelial cells (HAECs) were purchased as cryopreserved samples of third passage (Lot: 3F1346) from Cambrex (Wakersville, MD, USA). The HAECs were subcultured once and stored in liquid nitrogen until cell culture experiment. The HAECs used in the experiment were fourth passage. Each well of a 12-well plate of polystyrene (Iwaki) was filled with 1 mL of a supplemented culture medium (EGM-2; Lot: 08103123, Cambrex) and equilibrated at 37 °C in a humidified incubator under 5% CO_2 for 30 min before cell seeding. After the frozen cells were thawed at 37 °C, 10 μL of the cell suspension was seeded in each well. The initial cell density was 2.2×10^3 cells·cm^{-2}. Cell viability assessed by the trypan blue exclusion test was 83% for the cell suspension. The cell seeded plates were placed in a humidified incubator at 37 °C under 5% CO_2. The HAECs were cultured for 48 h. Cell culture mediums were replaced with fresh medium 24 h after cell seeding. At 48 h after cell seeding, cell culture mediums were each replaced with an aqueous suspension of copolymer **8**. Then the HAECs were cultured in the polymer suspension for 1, 6, and 24 h in a humidified incubator at 37 °C under 5% CO_2 to study cellular uptake of nanoaggregates of copolymer **8**. For fluorescence microscopy observation, the cells were fixed by immersion in 10% formaldehyde neutral buffer solution (Nacalai Tesque) at room temperature (22 °C) for 15 min and were washed three times with phosphate-buffered saline (PBS; Gibco). Fluorescence images of the cells were taken with a fluorescence microscope (IX71; Olympus) equipped with a CCD camera (DP70; Olympus). Fluorescence intensity of the incorporated copolymer **8** was measured by integrating the fluorescence intensity observed at each pixel of the fluorescence images using image analysis software (Fluoview ver. 5.0; Olympus).

Measurements

NMR spectra were recorded on a JEOL ECA 600 spectrometer. Optical rotations were measured with a Jasco P-1030 digital polarimeter. GPC analyses were performed by using a TOSOH 8012 with refractive index detection under the following conditions: Shodex Asahipak GF-310HQ column with water as eluent at a flow rate of 0.5 mL·min^{-1}. The calibration curve was obtained using pullulan standards. CD and UV-vis spectra were measured in a quartz cell (thickness 1 cm) at room temperature using a Jasco J-820 spectropolarimeter and Shimadzu UV160A spectrophotometer, respectively. The SEM images were obtained using a Hitachi S-4100 electron microscope. The DLS measurement was performed on a Zetasizer 3000 (Malvern Instruments). Fluorescence spectra were obtained on a fluorescence spectrometer (Shimadzu) using a quartz cuvette (1-mm path length).

Results and Discussion

Copolymerization of 1 with 5

The polymerization of monosubstituted acetylene derivatives has been widely investigated using Rh complex catalysts, which enables stereoselective synthesis of the corresponding polyacetylenes of the *cis*-isomers.[16] As

already reported in our previous publication, **1** was polymerized using (nbd)Rh$^+$ B$^-$(C_6H_5)$_4$ as the catalyst at around 25 to 50 °C in a mixed solvent of THF and water (9:1, v/v).[12] In this study, we performed the copolymerization of **1** with **5** under similar conditions. The copolymerization with various feed ratios of **1** to **5** was carried out using the Rh catalyst (5.0 mol-% for **1** + **5**) at 30 °C in a THF-water mixed solvent under argon. After polymerization, the resulting mixture was concentrated and then dissolved in DMSO. The solution was poured into a large amount of methanol to precipitate the polymeric product. The precipitate was isolated by filtration and dried under reduced pressure to give the copolymer **6** (Table 1). The copolymer was soluble in water and DMSO, and its $\overline{M}_n$ value was estimated by GPC analysis with water as eluent using pullulan standards. Figure 1a shows the ^{1}H NMR spectrum of the copolymer (entry 1, Table 1) measured in DMSO-d_6. The signals due to the sugar and alkyl protons are observed at around δ 3.0–4.3 (signals **e**–**h**) and δ 0.84, 1.21, 1.45, 2.15 (signals **a**–**d**), respectively. In addition to these signals, signal **i** ascribed to the main-chain proton of –CH=C– appears centered at δ 6.11. The chemical shift of this signal realistically corresponds to the *cis*-isomer. Furthermore, there is no signal due to the *trans*-isomer at lower magnetic field from the *cis*-signal. The NMR results support structure **6** as that of the copolymer, which is mainly composed of *cis*-isomer. The unit ratio of the copolymer is calculated by the integrated ratio of signal **a** and signal **i**.

Table 1 shows the copolymerization results obtained by the various feed ratios of **1** to **5**. The yields and the $\overline{M}_n$ values are 57.0–78.1% and 5 200–9 700, respectively. The unit ratios of **5** in the copolymers increase with increasing molar ratios of **5** in the feeds. In all cases, however, the ratios of **5** in the copolymers are lower than those in the feeds. This is probably because the copolymers with higher

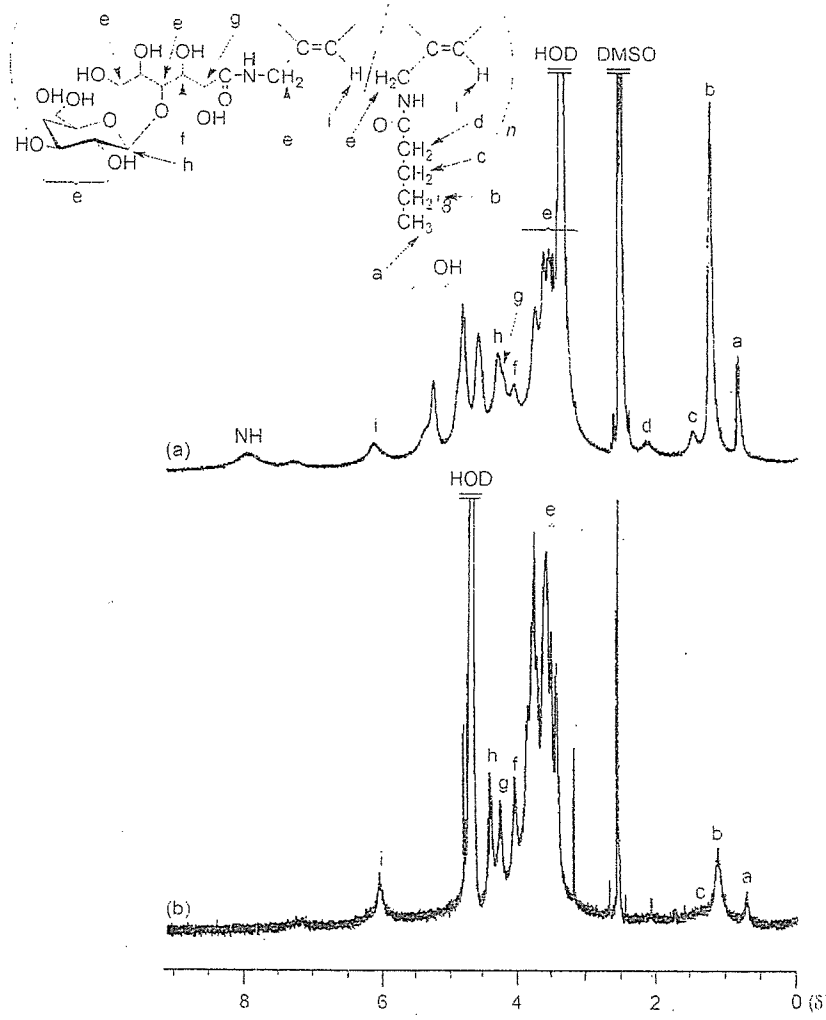

Figure 1. ^{1}H NMR spectra of copolymer **6** (entry 1, Table 1) in DMSO-d_6 (a) and D_2O (b).

contents of the unit **5** are lost as methanol-soluble fractions during the isolation procedure. The optical rotations of the copolymers with the higher contents of the sugar units were larger than those with the lower contents.

Formation of Molecular Aggregates in Water

When the copolymerization was followed by thin-layer chromatography (TLC) on silica gel (methanol: chloroform = 2:1 for **1**; hexane: ethyl acetate = 1: 1 for **5**), **1** appeared to be consumed at the early stage of the reaction; subsequently, the consumption of **3** at a later stage was confirmed. This indicated that **6** had the block copolymeric sequence between the unit **1** and the unit **5** rather than in random style. In fact, the intensities of the alkyl signals **a–d** in the ^{1}H NMR spectrum of **6** in D_2O (Figure 1b) are obviously lower than those of the same copolymer measured in DMSO-d_6 (Figure 1a). The NMR results suggest formation of micelle-like aggregates having the outer hydrophilic sugar residues and the inner hydrophobic lauryloyl groups in water, and this was attributed to the block copolymeric sequence. The formation of molecular aggregates of **6** in water was also confirmed by the GPC measurements on aqueous solutions of **6** (entry 5, Table 1, the unit ratio of **1** to **5** = 1.0:0.26) ranging in concentration from 0.05 to 9.0 mg · mL^{-1}. Figure 2 shows the relations of the $\overline{M}_n$ values to the sample concentrations in the GPC experiments. The $\overline{M}_n$ values increase from ca. 6300 to ca. 11000 for concentrations higher than 0.70 mg · mL^{-1}. These data suggest the formation of molecular aggregates for the higher concentrations of **6** in water. The molecular aggregates of **6** were directly observed by SEM. The SEM image of the spin-coated sample from the aqueous solution of **6** (entry 4, Table 1, the unit ratio of **1** to **5** = 1.0:0.32) on aluminium plate (Figure 3) shows the particle-type molecular aggregates with average diameters of 20–40 nm. The particle sizes were also confirmed by DLS measurement. The mean particle diameter of the sample shown as entry 4 in Table 1 was 85.2 ± 14.1 nm. The difference in the aggregate sizes obtained by SEM and DLS can be attributed to the difference in the sample condition: dry for SEM and wet for DLS.

Secondary Conformation of 6

We already reported in our previous report that the CD spectrum of the homopolymer **2** in water showed the positive Cotton effect at 330 nm corresponding to the main-chain UV-vis absorption.[11,12] This indicated the possibility for formation of a one-handed helical conformation in the main chain of **2**. In this study, the CD analysis was also performed to reveal the secondary conformation of copolymer **6**. Figure 4 shows the CD spectra of **6** (entry 5, Table 1, unit ratio of **1** to **5** = 1.0:0.26) in comparison with those of copolymer **4** (unit ratio of **1** to **3** = 1.0: 0.39) measured in DMSO and water at room temperature. The CD spectrum of **6** in DMSO (Figure 4a) shows the positive Cotton effect at 360 nm, corresponding to the main-chain UV-vis absorption. The positive Cotton effect also appeared at this region in the CD spectrum in water (Figure 4b), although its intensity was lower than that in DMSO. It has been reported that the helical structure of poly(*N*-propargylamide)s is stabilized by the intramolecular hydrogen bonds between the pendant amide groups.[17] In polar solvents such as DMSO and water, therefore, the hydrogen bonds are readily broken to effect destabilization of the helical structure. The helical conformation of **6** in polar solvents is probably stabilized by the bulky substituents in the side chains of sugar and lauryloyl groups. These bulky groups shield the hydrogen bonds from the solvents, which consequently stabilizes the helical structure. This reasoning is also supported by comparison of the CD spectra of copolymer **4** (gray lines in

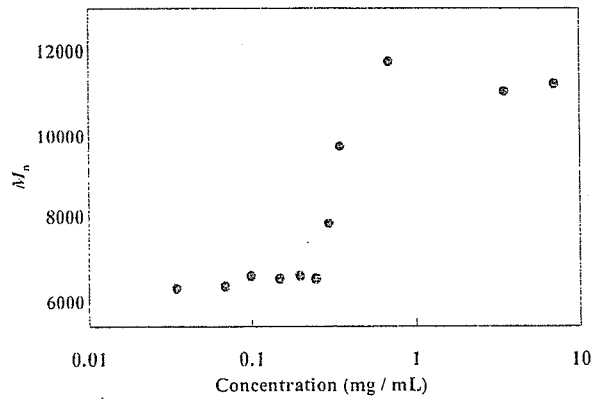

Figure 2. $\overline{M}_n$ values versus sample concentrations in GPC measurements with water as eluent (entry 5, Table 1).

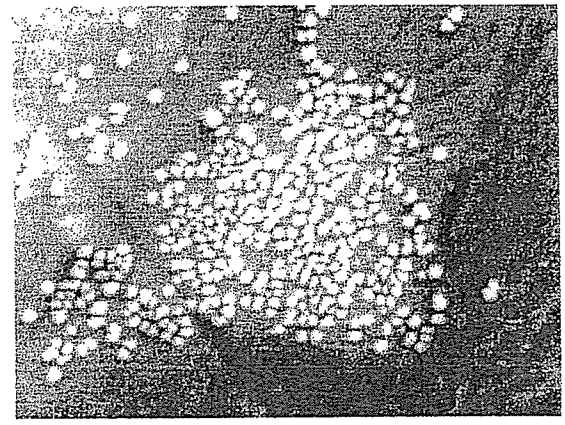

Figure 3. SEM image of **6**; the sample was prepared by spin coating of the dispersed solution of **6** (entry 4, Table 1) in water.

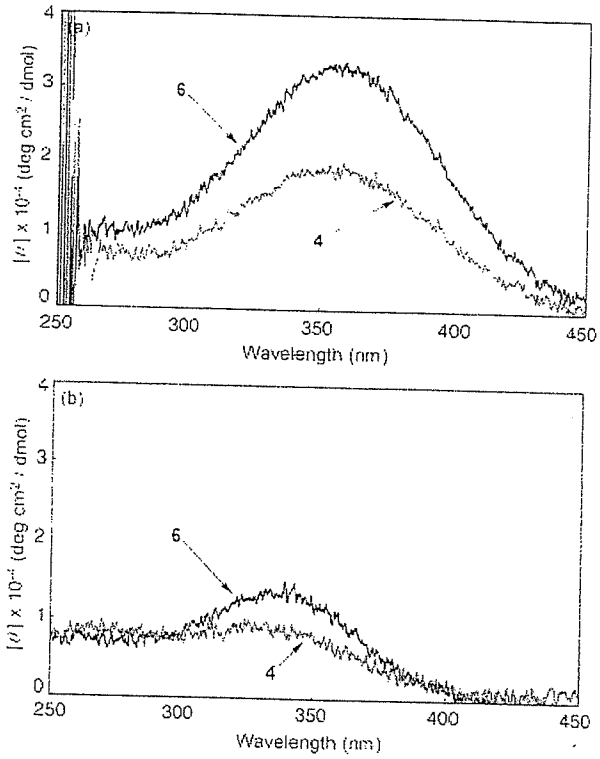

Figure 4. CD spectra of **6** (entry 5, Table 1, unit ratio: 1:5 1.0:0.26) and **4** (unit ratio: 1:3 1.0:0.39) in DMSO (a) and water (b) (c 0.2 mmol · L^{-1}).

Figure 4a, b), which has the less bulky hexanoyl groups. The CD spectra of **4** show weaker Cotton effects than those of **6**, indicating the stabilization of the helical conformation as a result of the bulkiness of the pendant groups.

Cellular Uptake of Amphiphilic Copolymer 8

To evaluate cell uptake of the copolymer by fluorescence microscopy, the rhodamine B dye moiety was introduced into the amphiphilic copolymer. First, an *N*-propargylamide derivative **7** having a pendant rhodamine B moiety was prepared by condensation of *N*-propargylamine hydrochloride with rhodamine B in the presence of a condensing agent (1-[(3-dimethylamino)propyl]-3-ethylcarbodiimide hydrochloride) in methanol. Then, the isolated **7** was copolymerized with **1** and **5** under conditions similar to those described above (Scheme 3). Although **7** did not have homopolymerizability by Rh catalyst, the unit from **7** was slightly incorporated into the resulting terpolymer by the copolymerization. The existence of the rhodamine B moiety in the obtained terpolymer **8** was confirmed by appearance of the signals due to methyl protons of N-CH_2CH_3 as well as the aromatic protons in the ^{1}H NMR spectrum of the product. However, the intensities of the signals were too weak to determine the exact content of the dye moiety in the copolymer by the integration ratio. For comparison, hydrophilic copolymer **9** was synthesized by copolymerization of monomer **1** with monomer **7** using Rh catalyst (Figure 5).

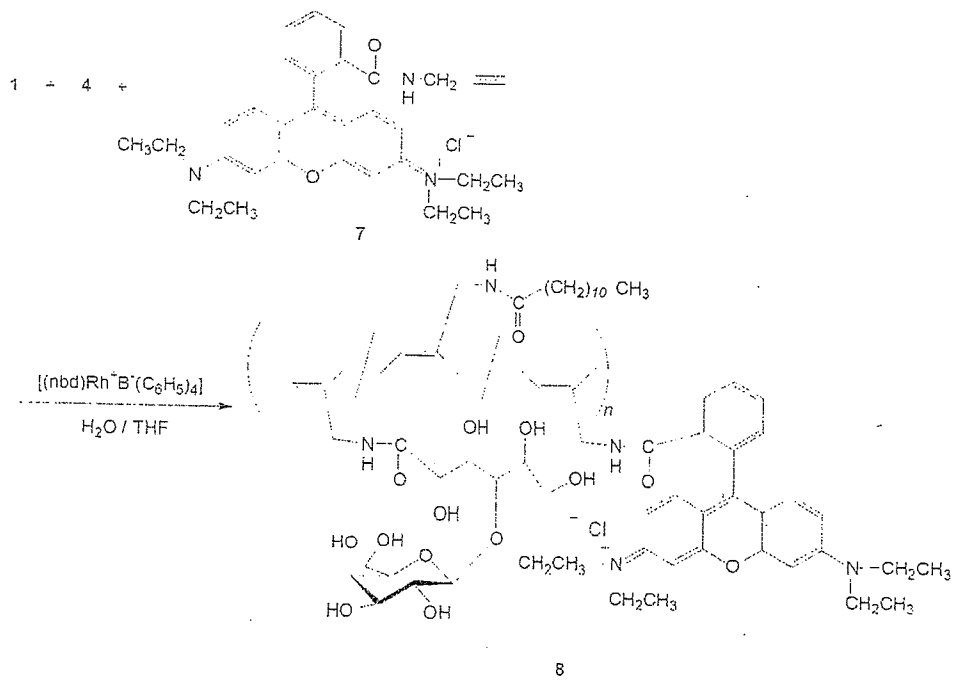

Scheme 3. Terpolymerization of **1**, **5**, and **7**.

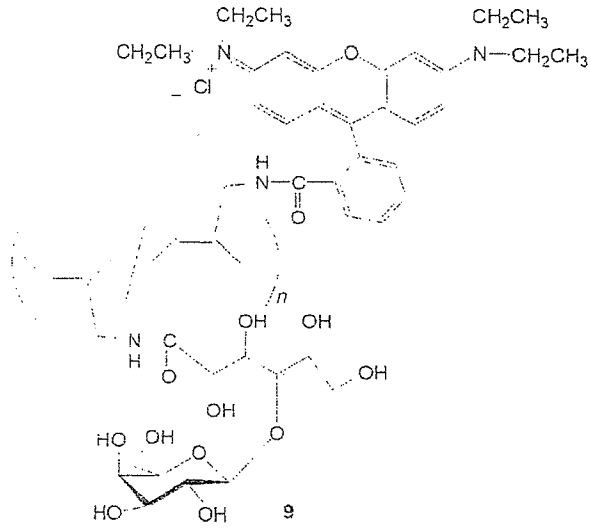

Figure 5. Structure of copolymer 9.

The cell uptake of terpolymer 8 was studied by culturing human aortic endothelial cells (HAECs) in a culture medium containing the terpolymer 8. Ten milligrams of 8 was suspended in 10 mL of culture medium EGM-2 and stirred for 3 h at room temperature. The suspension of 8 was sonicated at 25 W and 40 kHz for 5 min in an ultrasonic bath. The sonication was repeated twice. The obtained suspension was filtered through membrane filters with the pore sizes of 0.45 μm and 0.2 μm for sterilization. An aqueous solution of polymer 9 was prepared by following the above procedure. To evaluate the concentration of 8, a calibration curve (data not shown) was obtained by using the aqueous solution of 9 (1 mg · mL^{-1}) as a standard polymer sample to relate concentration to fluorescence intensity. The concentration of 8 was estimated to be 0.09 mg · mL^{-1} by using the calibration curve. The DLS measurement revealed that the polymer aggregates (nanoparticles) of 8 have a mean diameter of 114.9 ± 32 nm in a culture medium containing 10% bovine serum. HAECs were exposed to the polymer aggregates of 8 while they were cultured in the culture medium containing the amphiphilic polymer 8. After the prescribed period of culture, 1, 6, or 24 h, the HAECs were fixed in 10% formaldehyde neutral buffer solution for microscope observation. Figure 6 shows phase contrast (a), fluorescence (b), and merged (phase contrast + fluorescence) (c) images of HAECs after 24 h of incubation. The merged image demonstrates that red fluorescent light of rhodamine B was emitted from the sites where HAECs were located. This indicates that the polymer aggregates of 8 were incorporated into HAECs. The fluorescence images at each time of incubation are shown in Figure 7. The fluorescence images get brighter with the incubation time. To quantitatively evaluate cell uptake of nanoaggregates, fluorescence intensity per image (1 360 × 1 024 pixels) was determined by integrating the brightness at each pixel of the fluorescence image using image analysis software. The

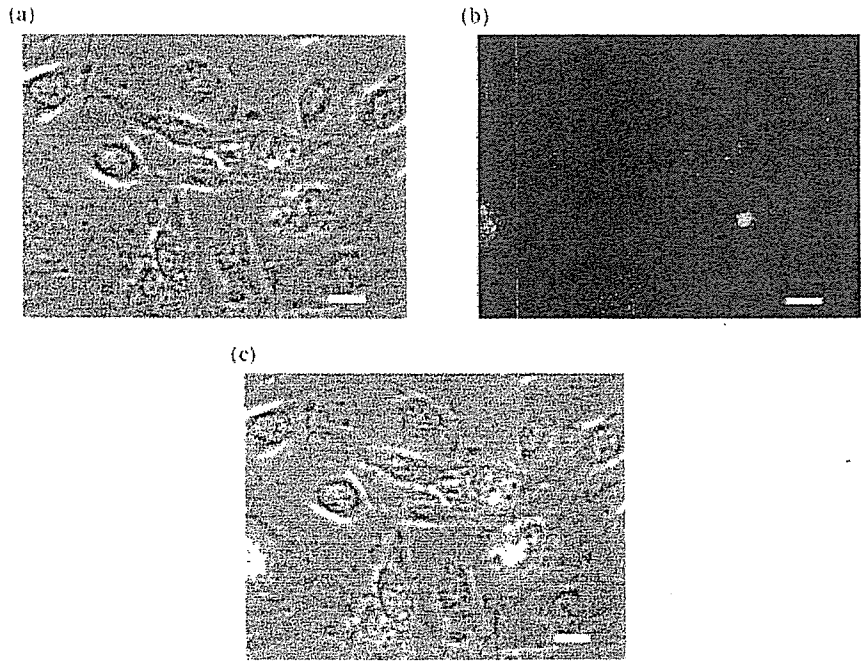

Figure 6a–c. Localization of rhodamine B-labeled copolymer 8 in human aortic endothelial cells. Phase contrast image (a), fluorescence image (b), and merged image of (a) and (b). Bars: 20 μm.

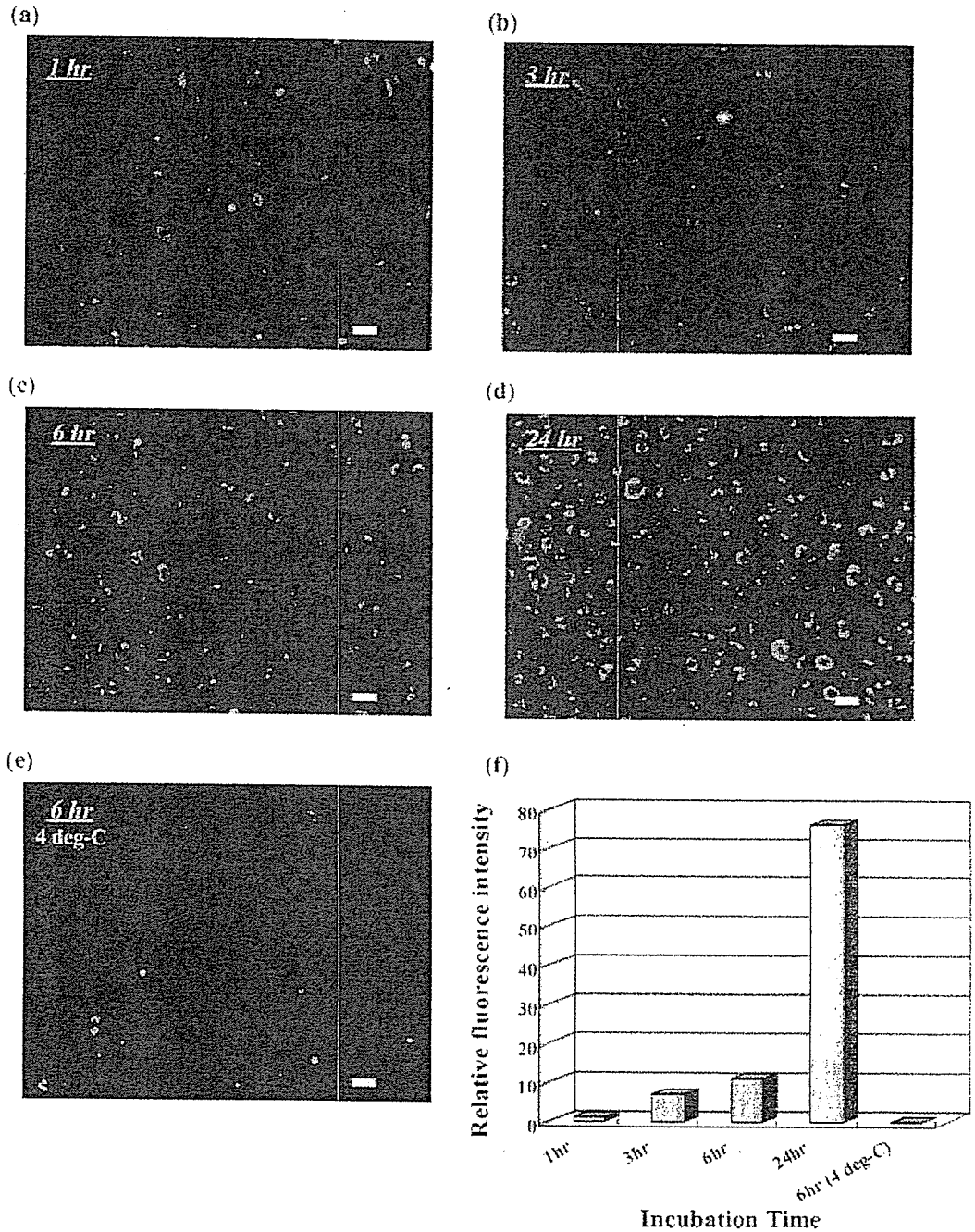

Figure 7a–f. Uptake of rhodamine B-labeled copolymer **8** by human aortic endothelial cells: incubation time, 1 h (a), 3 h (b), 6 h (c), 24 h (d) (incubation at 37 °C), and 6 h (incubation at 4 °C) (e). Bars: 20 μm; The uptake is quantitatively represented as relative fluorescence intensity in the bar graph (f).

fluorescence intensity was normalized in a ratio of the fluorescence intensity at each incubation time to that at 1 h of incubation. The ratio was termed as the relative fluorescence intensity. The time course of the relative fluorescence intensity is shown in Figure 7f and indicates that HAECs incorporated progressively more nanoaggregates of **8** during the incubation time. The relative fluorescence intensity was 7-fold at 3 h, 11-fold at 6 h, and 76-fold at 24 h of incubation. In contrast, the relative fluorescence intensity dropped considerably and was only 12% of the control level (1 h at 37 °C) when HAECs were exposed to the nanoaggregates of **8** at 4 °C for 6 h. The fact that the temperature triggered a dramatic decrease in the relative fluorescence intensity suggests that the nanoag-

gregates are incorporated into HAECs by endocytosis. Endocytosis is known as a cellular process that is coupled with temperature-dependent metabolic activities.[18] Furthermore, it is known that some receptors and membrane microdomains of endothelial cell are involved in endocytosis.[19] However, it is not clear which of the endocytic pathways is responsible for the uptake of the nanoaggregates. This issue is now under investigation.

Conclusion

In this study, we investigated synthesis of the amphiphilic poly(*N*-propargylamide) **6** containing both sugar residues (hydrophilic part) and long alkyl chains (hydrophobic part) in order to develop a novel nanoaggregate based on the self-organization of amphiphilic polymers with rigid backbone. The desired polymer was prepared by copolymerization of the two *N*-propargylamide monomers **1** and **5** having a galactose residue and a lauryloyl group, respectively, catalyzed by a Rh complex. The GPC, ^{1}H NMR, SEM, and DLS analyses of the resulting copolymers indicated formation of the nanoparticles in water. The formation of the one-handed helical conformation of the copolymer in both DMSO and water was confirmed by the CD spectra. An amphiphilic poly(*N*-propargylamide) containing fluorescent dyes was newly designed to evaluate cell uptake of nanoparticles of the amphiphilic copolymer by fluorescence microscopy. The *N*-propargylamide monomer **7**, having a rhodamine B dye moiety, was prepared and copolymerized with **1** and **5**. Human aortic endothelial cells (HAECs) were cultured in a medium containing the fluorescent-dye-labeled amphiphilic copolymer. Cell uptake of the copolymer was confirmed by red fluorescence emission from each of the HAECs. Progressive uptake was observed during the incubation period. When the cell culture experiment was conducted at 4 °C, the fluorescence intensity of the red emission was considerably lowered. This indicates that the cell uptake is inhibited at 4 °C and that this uptake process should occur in an endocytic pathway rather than by simple adsorption to the plasma membrane of HAECs. We are now synthesizing a fluorescent-dye-labeled hydrophilic copolymer of monomer **1** with monomer **7** to study preferential cell uptake of the nanoaggregates of the amphiphilic copolymer. In the future, we anticipate that nanoparticles will be able to be preferentially endocytosed into cells rather than monomeric chains of water-soluble copolymer. If this does occur, the nanoparticles of the amphiphilic copolymer will be a promising nanocarrier for drug delivery.

Acknowledgements: This work was financially supported by the *Asahi Glass Foundation*. The author (T. N.) thanks Professor *Mitsuru Akashi* of Osaka University and Dr. *Takami Akagi* of the Japan Science and Technology Agency for dynamic light scattering measurement. The author (T. N.) thanks Dr. *Tetsuji Yamaoka* and Dr. *Atsushi Mahara* of the National Cardiovascular Center Research Institute for fluorescence spectroscopy analysis.

[1] M. Okada, *Prog. Polym. Sci.* **2001**, *26*, 67.
[2] Y. C. Lee, R. T. Lee, "*Neoglycoconjugates: Preparation and Applications*", Academic Press, San Diego **1994**.
[3] K. Kobayashi, A. Tsuchida, T. Usui, T. Akaike, *Macromolecules* **1997**, *30*, 2016.
[4] K. Kobayashi, N. Kakishita, M. Okada, T. Akaike, T. Usui, *J. Carbohydr. Chem.* **1994**, *13*, 753.
[5] L. L. Kiessling, N. L. Pohl, *Chem. Biol.* **1996**, *3*, 71.
[6] M.-G. Baek, R. C. Stevens, D. H. Charych, *Bioconjugate Chem.* **2000**, *11*, 777.
[7] I.-B. Kim, B. Erdogan, J. N. Wilson, U. H. F. Bunz, *Chem. Eur. J.* **2004**, *10*, 6247.
[8] T. Hasegawa, S. Kondoh, K. Matsuura, K. Kobayashi, *Macromolecules* **1999**, *32*, 6595.
[9] J. Kadokawa, Y. Shinmen, S. Shoda, *Macromol. Rapid Commun.* **2005**, *26*, 103.
[10] A. Takasu, K. Iso, T. Dohmae, T. Hirabayashi, *Biomacromolecules* **2006**, *7*, 411.
[11] K. Matsuura, S. Furuno, K. Kobayashi, *Chem. Lett.* **1998**, 847.
[12] J. Kadokawa, K. Tawa, M. Suenaga, Y. Kaneko, M. Tabata, *J. Macromol. Sci., Pure Appl. Chem.* **2006**, *43*, 1179.
[13] J. Deng, J. Tabei, M. Shiotsuki, F. Sanda, T. Masuda, *Macromolecules* **2004**, *37*, 9715 and references therein.
[14] R. R. Shrock, J. A. Osborn, *Inorg. Chem.* **1970**, *9*, 2339.
[15] J. Deng, J. Tabei, M. Shiotsuki, F. Sanda, T. Masuda, *Macromolecules* **2004**, *37*, 1891.
[16] M. Tabata, T. Sone, Y. Sadahiro, *Macromol. Chem. Phys.* **1999**, *200*, 265.
[17] J. Tabei, R. Nomura, T. Masuda, *Macromolecules* **2002**, *35*, 5405.
[18] G. Durin, S. Cottin, E. Blanc, A. R. Rees, *J. Temsamani, J. Biol. Chem.* **2003**, *278*, 31192.
[19] S. Muro, M. Koval, V. Muzykantov, *Curr. Vasc. Pharmacol.* **2004**, *2*, 281.

Cardiovasc Drugs Ther (2006) 20: 159–165
DOI 10.1007/s10557-006-8285-8

BASIC RESEARCH

Granulocyte Colony-Stimulating Factor Mediates Cardioprotection Against Ischemia/Reperfusion Injury via Phosphatidylinositol-3-Kinase/Akt Pathway in Canine Hearts

Hiroyuki Takahama · Tetsuo Minamino · Akio Hirata · Akiko Ogai · Hiroshi Asanuma · Masashi Fujita · Masakatsu Wakeno · Osamu Tsukamoto · Ken-ichiro Okada · Kazuo Komamura · Seiji Takashima · Yoshiro Shinozaki · Hidezo Mori · Naoki Mochizuki · Masafumi Kitakaze

Published online: 16 June 2006

Abstract
Purpose Recent studies suggest that G-CSF prevents cardiac remodeling following myocardial infarction (MI) likely through regeneration of the myocardium and coronary vessels. However, it remains unclear whether G-CSF administered at the onset of reperfusion prevents ischemia/reperfusion injury in the acute phase. We investigated acute effects of G-CSF on myocardial infarct size and the incidence of lethal arrhythmia and evaluated the involvement of the phosphatidylinositol-3 kinase (PI3K) in the *in vivo* canine models.
Methods In open-chest dogs, left anterior descending coronary artery (LAD) was occluded for 90 minutes followed by 6 hours of reperfusion. We intravenously administered G-CSF (0.33 μ/kg/min) for 30 minutes from the onset of reperfusion. Wortmannin, a PI3K inhibitor, was selectively administered into the LAD after the onset of reperfusion.
Results G-CSF significantly ($p < 0.05$) reduced myocardial infarct size (38.7±4.3% to 15.7±5.3%) and the incidence of ventricular fibrillation during reperfusion periods (50% to 0%) compared with the control. G-CSF enhanced Akt phospholylation in ischemic canine myocardium. Wortmannin blunted both the infarct size-limiting and anti-arrhythmic effects of G-CSF. G-CSF did not change myeloperoxidase activity, a marker of neutrophil accumulation, in the infarcted myocardium.
Conclusion An intravenous administration of G-CSF at the onset of reperfusion attenuates ischemia/reperfusion injury through PI3K/Akt pathway in the *in vivo* model. G-CSF administration can be a promising candidate for the adjunctive therapy for patients with acute myocardial infarction.

Takahama and Hirata contributed equally to this work.

H. Takahama · A. Ogai · H. Asanuma · M. Wakeno · K. Komamura · H. Mori · M. Kitakaze
Department of Cardiovascular Medicine,
National Cardiovascular Center,
Suita 565-8565, Osaka, Japan

H. Takahama · M. Wakeno · N. Mochizuki
Department of Structural Analysis,
National Cardiovascular Center,
Suita 565-8565, Osaka, Japan

H. Takahama · M. Wakeno · N. Mochizuki
Department of Bioregulatory Medicine,
Osaka University Graduate School of Medicine,
Suita 565-0871, Osaka, Japan

T. Minamino (✉) · A. Hirata · M. Fujita · O. Tsukamoto · K.-i. Okada · S. Takashima
Department of Cardiovascular Medicine,
Osaka University Graduate School of Medicine,
2-2 Yamadaoka, Suita 565-0871, Osaka, Japan
e-mail: minamino@medone.med.osaka-u.ac.jp

Y. Shinozaki
Department of Physiological Science,
Tokai University School of Medicine,
Isehara 259-1193, Kanagawa, Japan

Key words G-CSF · myocardial infarction · ischemia-reperfusion injury · ventricular fibrillation · phosphatidylinositol-3 kinase · Akt

Abbreviations

VF	ventricular fibrillation
G-CSF	granulocyte colony-stimulating factor
WTMN	wortmannin

Introduction

Granulocyte colony-stimulating factor (G-CSF), a 20-kDa glycoprotein, promotes the proliferation, survival and differentiation of hematopoietic cells [1]. Furthermore, G-CSF can mobilize hematopoietic stem cells from bone marrow [2, 3]. Thus, G-CSF is believed to improve cardiac remodeling after myocardial infarction (MI) through regeneration of the myocardium and angiogenesis [4, 5]. In addition to these effects of G-CSF, Komuro and colleagues clearly demonstrated that the high dose of G-CSF acutely reduces infarct size by preventing apoptosis in the isolated hearts [6]. However, it remains unclear whether clinically relevant dosages of G-CSF can reduce the infarct size in the in vivo model and, if so, it is not clear which downstream signaling pathway is involved in the acute cardioprotective effects of G-CSF. Furthermore, although lethal arrhythmias are a major cause of death in patients with acute myocardial infarction [7, 8], anti-arrhythmic effects of G-CSF have not been determined.

Thus, we investigated the acute effects of a clinical relevant dose of G-CSF on ischemia/reperfusion injury including both lethal arrhythmias and infarct size in canine hearts. We also examined a role of the PI3K/Akt pathway, a down stream of G-CSF receptors, in the cardioprotective effects of G-CSF. In the present study, we adopted ischemia/reperfusion protocols that have not been tested in previous studies [4, 5], because coronary revascularization has been established as a standard therapy to attenuate cardiac damage after MI.

Materials and methods

Materials

G-CSF was provided by Kirin brewery company (Tokyo, Japan). Recombinant human G-CSF can increase the number of white blood cells in dogs [9]. Wortmannin was obtained from Sigma (St. Louis, MO), and antibodies against Phospho-Akt and Akt were obtained from Cell signaling technologies (Beverly, MA).

Instrumentation

Twenty-nine beagle dogs (Kitayama Labes, Gifu, Japan) weighing 8 to 12 kg were anesthetized by an intravenous injection of sodium pentobarbital (30 mg/kg), intubated and ventilated with room air mixed with oxygen (100% O_2 at flow rate of 1.0 to 1.5 l/min). Thoracotomy was done at the fifth left intercostal space, and the heart was suspended in a pericardial cradle. After intravenous administration of heparin (500 U/kg), the left anterior descending coronary artery (LAD) was cannulated for perfusion with blood from the left carotid artery through an extracorporeal bypass tube. This allows the selective infusion of drugs into the LAD-perfused areas through this bypass tube. The left atrium was catheterized for microsphere injection to measure myocardial collateral blood flow during ischemia as described previously [10]. Hydration was maintained by a slow normal saline infusion. Both systemic blood pressure (SBP) and heart rate (HR) were monitored continuously during the study. All procedures were performed in conformity with the Guide for the care and use of laboratory animals (NIH Publication No. 85–23, 1996 revision), and were approved by the *Osaka University Committee for Laboratory Animal Use.*

Experimental protocols

Protocol 1. Acute effects of G-CSF on infarct size and lethal arrhythmias in canine hearts

After hemodynamic stabilization, we intravenously administered either saline (Control group; $n = 9$) or G-CSF (0.33 μg/kg/min) (G-CSF group; $n = 6$) for 30 min following the onset of reperfusion. An intracoronary administration of wortmannin (WTMN), a PI3K inhibitor, was selectively administered into the LAD (1.5 μg/kg/min) for 60 min after the onset of reperfusion (GCSF + WTMN group, $n = 7$; WTMN group, $n = 7$) (Fig. 1). We have previously confirmed that the dose of wortmannin used prevents the phosphorylation of Akt in myocardium [10]. We measured infarct size and myocardial collateral blood flow during ischemia. In brief, infarct size was evaluated at the end of the protocol by Evans blue/TTC staining. Collateral blood flow during 90 min of ischemia was assessed by the non-radioactive microsphere method [10]. We also counted

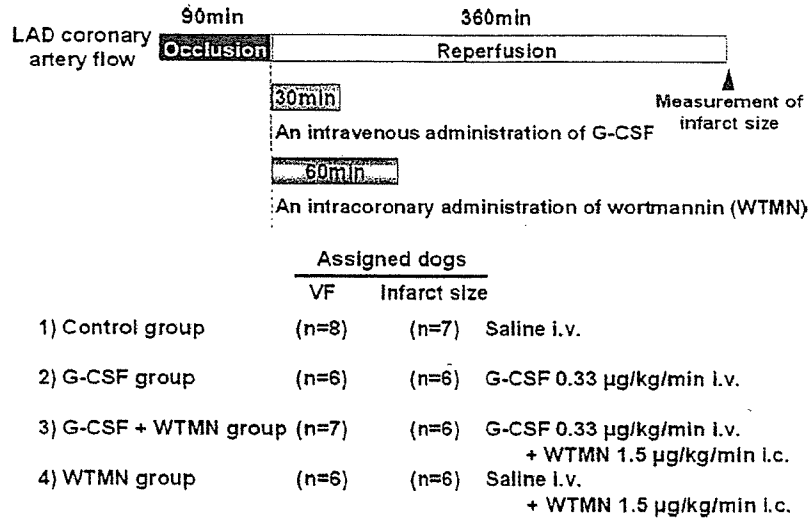

Fig. 1 Experimental protocols to assess myocardial infarct size and ventricular fibrillation (VF) in canine hearts. Myocardial infarct size was measured after 90 min of left anterior descending coronary artery (LAD) occlusion followed by 360 min of reperfusion. The incidence of VF was evaluated during reperfusion for 360 min. Intravenous administration of granulocyte colony-stimulating factor (G-CSF) was started at the onset of reperfusion and continued for 30 min. Intracoronary administration of wortmannin (WTMN) was started at the onset of reperfusion and continued for 60 min.

the incidence of VF during the 6 h reperfusion period (Fig. 1).

Finally, we measured myeloperoxidase (MPO) activity in LAD-perfused myocardium to check the accumulation of neutrophils in infarcted myocardium.

Protocol 2. Phosphorylation of Akt in ischemic myocardium

In this protocol, we used 11 dogs in Control group ($n = 3$), G-CSF group ($n = 4$), and G-CSF + WTMN group ($n = 4$). After 90 min of ischemia followed by 30 min of reperfusion, hearts were excised. The myocardial tissue in the ischemic zone, which was identified as the edge of the region showing necrosis, and non-ischemic zone were quickly placed into liquid nitrogen and stored at −80°C. Phosphorylation of Akt and total content of Akt were evaluated by immunoblotting as reported previously [10].

Immunoblotting

Immunoblotting was performed as described previously [11], and the immunoreactive bands were quantified by densitometry (Molecular Dynamics).

MPO activity

Several myocardial tissue samples were taken from the ischemic area in the dogs studied, frozen in liquid nitrogen and stored at −80°C until assay. The technical procedure has been described previously [12]. One unit of MPO activity was defined as that which degrades 1 μmol hydrogen peroxide per minute at 25°C.

Statistical analysis

Results are expressed as the mean ± SEM. Comparisons of the time course of the change in mean SBP and HR between groups were performed using two-way repeated measures analysis of variance (ANOVA). Comparisons of other data between groups were performed using one-way factional ANOVA. The Bonferroni-Holm procedure was used for correction of multiple comparisons [13]. The incidence of VF was compared using the χ^2-test and Fisher's exact probability test. A p value < 0.05 was considered to represent statistical significance.

Results

Criteria for exclusion

Since there was a negative correlation between myocardial collateral blood flow during ischemia and the incidence of VF [14, 15], it was important to assess myocardial collateral blood flow and exclude the dogs with high myocardial collateral blood flow. We excluded two dogs with excessive collateral blood flow (>15 ml/100 g/min) (Control group: 1, WTMN group: 1) among 29 dogs tested. Thus, 27 dogs were

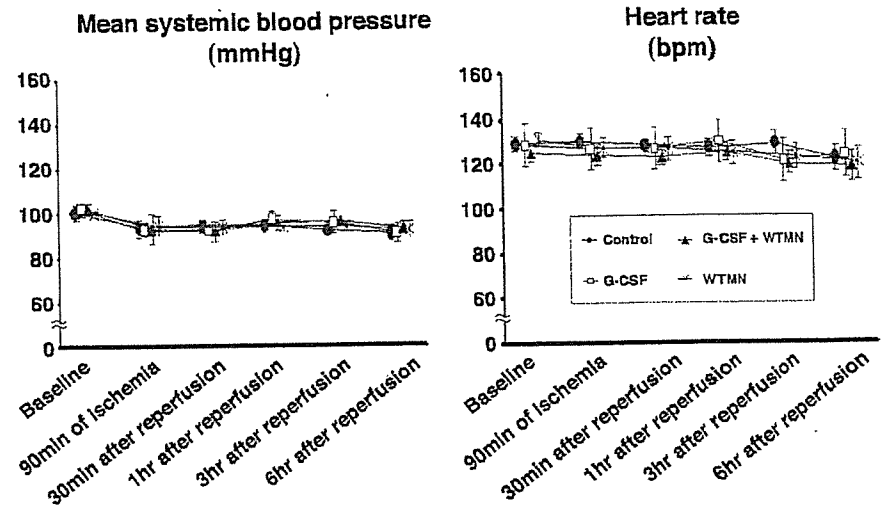

Fig. 2 The changes in mean systemic blood pressure (SBP) and heart rate (HR) during the experiment in groups tested. Neither SBP nor HR differed between the groups tested at baseline, 90 min of ischemia, at 30 min and 1, 3, and 6 h after reperfusion.

evaluated for VF analysis. Among these 27 dogs, we further excluded two dogs (Control group: 1, G-CSF + WTMN group: 1) from infarct size analysis that matched the exclusion criteria of lethal arrhythmia (more than two consecutive attempts required to convert VF with low-energy DC pulses applied directly to the heart) [10].

Effects of G-CSF on infarct size and VF during the reperfusion period

Throughout the study, neither SBP nor HR differed among the four groups (Fig. 2). The area at risk and myocardial collateral blood flow during myocardial ischemia were also comparable in the groups tested (Fig. 3). Figure 4 shows infarct size in the groups tested. G-CSF reduced ($p < 0.05$) infarct size compared with the control group. The intracoronary administration of wortmannin for 60 min after the onset of reperfusion abrogated the infarct size-limiting effects of G-CSF, although wortmannin alone did not affect infarct size.

G-CSF reduced ($p < 0.05$) the incidence of VF during the reperfusion period compared with the control group (Table 1). The antiarrhythmic effects of G-CSF were abolished by wortmannin.

Effect of G-CSF on MPO activity in infarcted myocardium

MPO activity in infarcted myocardium 6 h after reperfusion in G-CSF group did not differ from that in the control group. (10.0 ± 2.6 versus 10.7 ± 2.1 U/g protein).

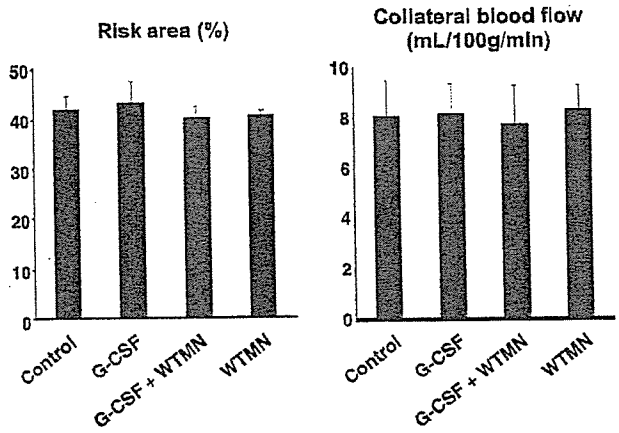

Fig. 3 Area at risk and myocardial collateral blood flow during ischemia in groups tested. Neither the area at risk nor myocardial collateral blood flow differed between the groups tested.

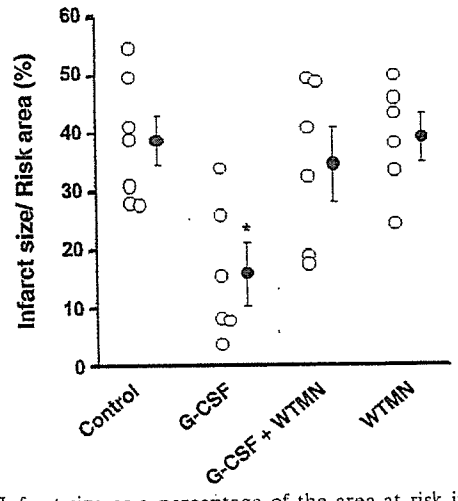

Fig. 4 Infarct size as a percentage of the area at risk in groups tested. Intravenous administration of G-CSF limited infarct size. The infarct-size limiting effect of G-CSF was blunted by the intracoronary administration of WTMN during reperfusion. *$p <$ 0.05 vs. control group.